Electronic Supplementary Material (ESI) for Dalton Transactions.


*Supplementary Information for:* **Studies of Hysteresis and Quantum Tunnelling of the Magnetisation in Dysprosium(III) Single Molecule Magnets**

Fabrizio Ortu, Daniel Reta, You-Song Ding, Conrad A. P. Goodwin, Matthew P. Gregson, Eric J. L. McInnes, Richard E. P. Winpenny, Yan-Zhen Zheng, Stephen T. Liddle, David P. Mills and Nicholas F. Chilton

## Experimental methods

### *General*

All syntheses and manipulations were conducted under argon with rigorous exclusion of oxygen and water using Schlenk line and glove box techniques. THF, toluene, benzene and hexane were dried by refluxing over potassium and stored over potassium mirrors (THF was stored over 4 Å molecular sieves). DCM was dried over $CaH_2$ and stored over or 4 Å molecular sieves. All solvents were degassed before use. Anyhdrous $DyCl_3$ and $YCl_3$ were purchased from Alfa Aesar and were used as received. $^{164}Dy_2O_3$ ($^{164}Dy$ isotopic content 96.80%) was purchased from Euriso-top and used as received to prepare $^{164}DyCl_3$ following literature procedures.[1] $NaBPh_4$ and $Na^tBuO$ were purchased from Sigma-Aldrich and used as received. $KCp^{ttt}$ (ref. [2]), $[H(SiEt_3)_2][B(C_6F_5)_4]$ (refs. [3] and [4]), $KCH_2Ph$ (ref. [5]) and $BIPMH_2$ (ref. [6]) were prepared according to literature methods. $^1H$ (400 MHz) NMR spectra were obtained on an Avance III 400 MHz spectrometer at 298 K. These were referenced to the solvent used, or to external TMS. $C_4H_8O$ and $C_6D_6$ were dried by refluxing over K and $CD_2Cl_2$ was dried by refluxing over $CaH_2$. All NMR solvents were vacuum transferred and degassed by three freeze-pump-thaw cycles before use. Crystals were screened with a Rigaku XtalLAB AFC11 diffractometer, equipped with CCD detector and a graphite-monochromated Mo $K_\alpha$ ($\lambda = 0.71073$ Å) or Cu $K_\alpha$ radiation ($\lambda = 1.54178$ Å). PXRD analysis are not possible using our apparatus for these highly air-sensitive samples. Elemental and ICP-OES analyses were performed by Mrs Anne Davies and Mr Martin Jennings at The University of Manchester. $^{164}Dy$-enriched samples were digested with $HNO_3$ and analysed by ICP-MS with an Agilent 7500cx by Mr Paul Lygoth at The University of Manchester. Magnetic measurements were performed with a Quantum Design MPMS-XL7 SQUID magnetometer. Freshly prepared crystalline samples (~30 mg) were crushed and loaded into an NMR tube along with ~15 mg powdered eicosane under an inert atmosphere, which was then evacuated and flame-sealed to a length of ~5 cm. The eicosane was melted by heating the tube gently with a low-power heat gun.

### *Synthesis*

***[Dy($^t$BuO)Cl(THF)$_5$][BPh$_4$] (1-Dy):*** Synthesis adapted from ref. [7] for $[Y(^tBuO)Cl(THF)_5][BPh_4]$ (see ref. [8]). A slurry of $DyCl_3$ (0.269 g, 1 mmol) in THF (15 mL) was added to a solution of $NaO^tBu$ (0.098 g, 1.02 mmol) and $NaBPh_4$ (0.349 g, 1.02 mmol) in THF (15 mL) at room temperature with stirring. The mixture was stirred (16 hours), forming a white suspension, and then allowed to settle (2 hours). The resulting suspension was filtered and the colourless solution concentrated (~2 mL) to afford crystals at room temperature. Yield: 0.228 g, 0.24 mmol, 24 %. Calcd (%) for $C_{48}H_{69}BClDyO_6$: C, 60.63; H, 7.31; Found: C, 57.19(28); H, 7.11(12) (standard deviation calculated over 5 measurements). The reproducibly low microanalysis carbon values could be attributed to carbide formation, however we note that due to the oxophilic nature of the $Dy^{3+}$ cation, any impurities in this sample are likely to be degradation products from the decomposition reaction of the complex with minor traces of oxygen or water, leading to hydrated $Dy^{3+}$ species: these would be paramagnetic impurities with minimal magnetic anisotropy and no magnetic hysteresis – thus they would not change the observed QTM step, nor the coercive field position, and would not affect the conclusions made in this paper. Several crystals of **1-Dy** were screened, giving the same unit cell parameters as $[Y(^tBuO)Cl(THF)_5][BPh_4]$ (ref. [7]) in every instance.

***Dy@[Y($^t$BuO)Cl(THF)$_5$][BPh$_4$] (1-Dy@Y and 1-$^{164}$Dy@Y):*** Synthesis adapted from refs. [7] and [8]. A slurry of $DyCl_3$ (0.014 g, 0.05 mmol) and $YCl_3$ (0.183 g, 0.97 mmol) in THF (15 mL) was added to a solution of $NaO^tBu$ (0.098 g, 1.02 mmol) and $NaBPh_4$ (0.349 g, 1.02 mmol) in THF (15 mL) at room temperature with stirring. The mixture was stirred (16 hours), forming a white suspension, and then allowed to settle (2 hours). The resulting suspension was filtered and the colourless solution concentrated (~2 mL) to afford crystals at room temperature.

***1-Dy@Y:*** 0.268 g, 0.30 mmol, 30 %. Calcd (%) for $C_{48}H_{69}BClDy_{0.05}O_6Y_{0.95}$: C, 65.45; H, 7.89; Found: C, 62.93(62); H, 7.08(15) (standard deviation calculated over 5 measurements). The reproducibly low microanalysis values are again attributed to a minor amount of sample decomposition (see **1-Dy** above). Y/Dy composition (ICP-OES): Y 94.4%, Dy 5.6%. Several crystals of **1-Dy@Y** were screened, giving the same unit cell parameters as $[Y(^tBuO)Cl(THF)_5][BPh_4]$ (ref. [7]) in every instance.

***1-$^{164}$Dy@Y:*** 0.331 g, 0.37 mmol, 37 %. Calcd (%) for $C_{48}H_{69}BClDy_{0.05}O_6Y_{0.95}$: C, 65.45; H, 7.89; Found: C, 65.68; H, 7.75. Y/Dy composition (ICP-OES): Y 94.4%, Dy 5.6%. Isotopic fingerprint (ICP-MS) for $^{164}$Dy sample: 96.62% $^{164}$Dy, 2.27% $^{163}$Dy, 0.64% $^{162}$Dy, 0.37% $^{161}$Dy, 0.05% $^{160}$Dy, 0.02% $^{158}$Dy, 0.03% $^{156}$Dy. NMR spectra for natural abundance and $^{164}$Dy samples matched that previously reported for $[Y(^tBuO)Cl(THF)_5][BPh_4]$ (ref. 7). Several crystals of **1-$^{164}$Dy@Y** samples were screened, giving the same unit cell parameters as $[Y(^tBuO)Cl(THF)_5][BPh_4]$ (ref. [7]) in every instance.

***Dy@[K(18-crown-6-ether)(THF)$_2$][Y(BIPM)$_2$] (2-Dy@Y and 2-$^{164}$Dy@Y):*** Synthesis adapted from ref. [9] for $[K(18\text{-crown-6-ether})(THF)_2][Y(BIPM)_2]$. THF (20 mL) was added to Dy@[Y(BIPM)(BIPM-H)] (1.456 g, 1.21 mmol) and $KCH_2Ph$ (0.158 g, 1.21 mmol) at –78 °C with stirring. The mixture was allowed to warm slowly to room temperature and then stirred (16 hours). A solution of 18-crown-6-ether (0.32 g, 1.21 mmol) in THF (10 mL) was added to the reaction mixture at room temperature and stirred for 16 hours to afford an orange solution with some white precipitate. The suspension was filtered through a glass sinter and concentrated to 4 mL, affording crystals at room temperature.

***2-Dy@Y:*** 0.362 g, 0.22 mmol, 18%. Calcd (%) for $C_{82}H_{116}Dy_{0.05}KN_4O_8P_4Si_4Y_{0.95}$: C, 59.55; H, 7.07; N, 3.39; Found: C, 55.20; H, 6.51; N, 3.21. Reproducibly low carbon values could be attributed to silicon carbide formation, as has previously been observed for silicon-rich organometallic complexes,[10,11] or again attributed to a minor amount of sample decomposition (see **1-Dy** above). Y/Dy composition (ICP-OES): Y 94.1 %, $^{164}$Dy 5.9 %. Several crystals of **2-Dy@Y** were screened, giving the same unit cell parameters as $[K(18\text{-crown-6-ether})(THF)_2][Y(BIPM)_2]$ (ref. [9]) in every instance.

***2-$^{164}$Dy@Y:*** 0.517 g, 0.31 mmol, 26%. Calcd (%) for $C_{82}H_{116}Dy_{0.05}KN_4O_8P_4Si_4Y_{0.95}$: C, 59.55; H, 7.07; N, 3.39; Found: C, 56.27; H, 6.56; N, 3.29. Reproducibly low carbon values are due to silicon carbide formation, as has previously been observed for silicon-rich organometallic complexes,[10,11] again attributed to a minor amount of sample decomposition (see **1-Dy** above) Y/Dy composition (ICP-OES): Y 92.7%, Dy 7.3%. Isotopic fingerprint (ICP-MS) for $^{164}$Dy sample: 96.70% $^{164}$Dy, 2.34% $^{163}$Dy, 0.59% $^{162}$Dy, 0.33% $^{161}$Dy, 0.03% $^{160}$Dy, 0.01% $^{158}$Dy, 0.01% $^{156}$Dy. NMR for natural abundance and $^{164}$Dy samples matched that previously reported for [K(18-crown-6-ether)(THF)$_2$][Y(BIPM)$_2$] (ref. 8). Several crystals of **2-$^{164}$Dy@Y** were screened, giving the same unit cell parameters as [K(18-crown-6-ether)(THF)$_2$][Y(BIPM)$_2$] (ref. [9]) in every instance.

***Dy@[Y(Cp$^{ttt}$)$_2$][B(C$_6$F$_5$)$_4$] (3-Dy@Y and 3-$^{164}$Dy@Y):*** Samples synthesised following ref. [12], employing Dy@[Y(Cp$^{ttt}$)$_2$Cl] (0.379 g, 0.64 mmol) and [(Et$_3$Si)$_2$H][B(C$_6$F$_5$)$_4$] (0.580 g; 0.64 mmol). Characterisation data for **3-Dy@Y** has been previously reported.[12] Yield of $^{164}$Dy sample (mono DCM): 0.652 g, 0.49 mmol, 77%. Analysis for $^{164}$Dy sample (mono DCM): Calcd (%) for $C_{58}H_{58}BF_{20}Dy_{0.05}Y_{0.95}\cdot CH_2Cl_2$: C, 53.55; H, 4.57; Found: C, 53.18; H, 4.45. Y/Dy composition (ICP-OES): Y 92.6%, Dy 7.4%. Isotopic fingerprint (ICP-MS) for $^{164}$Dy sample (mono DCM): 96.66% $^{164}$Dy, 2.25% $^{163}$Dy, 0.61% $^{162}$Dy, 0.35% $^{161}$Dy, 0.06% $^{160}$Dy, 0.04% $^{158}$Dy, 0.03% $^{156}$Dy. NMR spectra for natural abundance and $^{164}$Dy samples matched that previously reported for [Y(Cp$^{ttt}$)$_2$][B(C$_6$F$_5$)$_4$] (ref. [12]). Several crystals of both **3-Dy@Y** and **3-$^{164}$Dy@Y** were screened, giving the same unit cell parameters as [Dy(Cp$^{ttt}$)$_2$][B(C$_6$F$_5$)$_4$] (ref. [12]) in every instance.

***Dy@[Y(BIPM)(BIPM-H)]:*** THF (20 mL) was added to a mixture of $YCl_3$ (0.371 g, 1.9 mmol) and $DyCl_3$ (0.027 g, 0.1 mmol) and refluxed (2 hours). A solution of $KCH_2Ph$ (0.781 g, 6 mmol) was added dropwise at 0 °C, and the light orange mixture was stirred (0 °C, 2 hours). The solvent was removed *in vacuo*, toluene (40 mL) was added and the reaction mixture cooled to −78 °C. A solution of H$_2$-BIPM (2.01 g, 3.6 mmol) in toluene (10 mL) was added, the light yellow mixture was allowed to warm to room temperature and then stirred (16 hours). The resulting yellow suspension was filtered through a glass sinter and the solvent removed, affording a yellow powder. The solid residue was washed with hexane (3×20 mL) and dried *in vacuo* to give a beige powder. Yield of $^{164}$Dy sample: 1.456 g, 1.2 mmol, 60%. NMR spectra for natural abundance and $^{164}$Dy samples matched that previously reported for [Y(BIPM)(BIPM-H)] (ref. [9]).

***Dy@[Y(Cp$^{ttt}$)Cl]:*** Samples were synthesised following ref. [12], employing $DyCl_3$ (0.018 g, 0.07 mmol), $YCl_3$ (0.195 g, 1.0 mmol), and KCp$^{ttt}$ (0.573 g, 2.1 mmol). Yield of $^{164}$Dy sample: 0.253 g, 0.42 mmol, 42%.

*Computational*

We use the Gaussian09d[13] suite of programs to perform all geometry optimizations and calculation of vibrational modes, using the pure exchange-correlation PBE functional[14,15] and Grimme's dispersion corrections.[16] We replaced Dy(III) with Y(III) in the calculations to facilitate SCF convergence, and assign the isotopic mass of Y to be that of naturally abundant Dy. The 28 inner electrons of Y were described with the Stuttgart RSC 1997 effective core potential and the remaining valence electrons were described with the corresponding valence basis set.[17–19] For compounds **1** and **3**, the first coordination sphere atoms had the cc-pVTZ basis, and the rest of the atoms were described with the cc-pVDZ basis.[20,21] Due to the anionic nature of complex **2**, we added diffuse functions by using the aug-cc-pVDZ basis for the coordinating carbon atoms, nitrogen and phosphorous atoms, and the cc-pVDZ basis for the remaining atoms. Calculation of the hessian confirmed that all optimised structures correspond to a minimum in the potential energy surface, as all frequencies are positive and the force constants are close to zero.

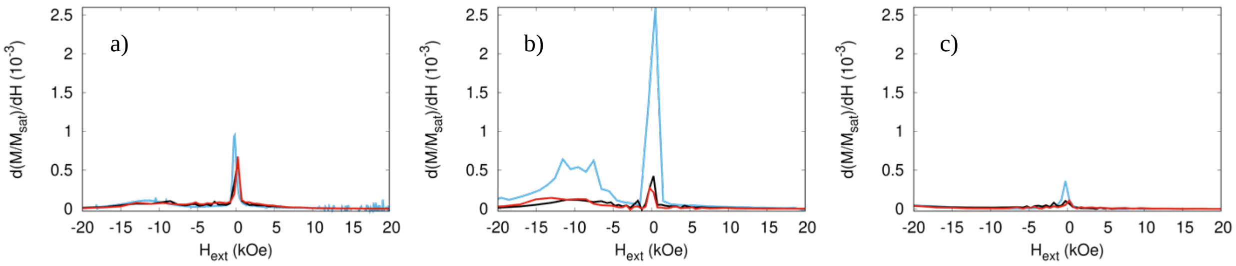


**Figure S1**. dM/dH curves from magnetic hysteresis measurements (Figure 1 main text) of **1** a), **2** b) and **3** c) at 2 K. Blue traces: naturally abundant Dy, undiluted; black traces: naturally abundant Dy, diluted ~5% in Y); red traces: ~96.6% $^{164}$Dy enriched, ~5% diluted in Y. For all data, except the blue traces for **1** and **2**, sweep rates are 110(20) Oe $s^{-1}$ for $|H_{ext}|$ > 20 kOe, 60(10) Oe $s^{-1}$ for 10 kOe < $|H_{ext}|$ < 20 kOe, 38(8) Oe $s^{-1}$ for 6 kOe < $|H_{ext}|$ < 10 kOe, and 20(4) Oe $s^{-1}$ for $|H_{ext}|$ < 6 kOe. For the blue trace for **1** the data are taken from main text ref. 26 with a sweep rate of 50 Oe $s^{-1}$, and for **2** the data are taken from main text ref. 24 with a sweep rate of 35 Oe $s^{-1}$.

**Table S1.** Generalised Debye model fit parameters for AC data for **1-$^{164}$Dy@Y**.

| **Temperature (K)** | **τ (s)** | **$\chi_S$ (emu)** | **$\chi_T$ (emu)** | **α** |
|---|---|---|---|---|
| 24.00022 | 6.18E-01 | 1.12E-06 | 4.13E-06 | 5.26E-01 |
| 26.0045 | 2.57E-01 | 1.09E-06 | 3.40E-06 | 4.53E-01 |
| 27.99879 | 1.46E-01 | 1.07E-06 | 2.98E-06 | 3.80E-01 |
| 29.99864 | 9.84E-02 | 1.01E-06 | 2.69E-06 | 3.45E-01 |
| 31.99858 | 7.42E-02 | 9.70E-07 | 2.51E-06 | 2.76E-01 |
| 33.99509 | 5.33E-02 | 9.13E-07 | 2.32E-06 | 2.91E-01 |
| 35.99602 | 3.97E-02 | 8.97E-07 | 2.18E-06 | 1.86E-01 |
| 37.99138 | 2.68E-02 | 8.40E-07 | 2.06E-06 | 2.91E-01 |
| 39.99168 | 1.69E-02 | 7.74E-07 | 1.90E-06 | 2.42E-01 |
| 41.99918 | 9.30E-03 | 7.38E-07 | 1.82E-06 | 2.29E-01 |
| 43.99891 | 4.53E-03 | 6.56E-07 | 1.72E-06 | 2.14E-01 |
| 46.00386 | 2.72E-03 | 6.56E-07 | 1.65E-06 | 1.78E-01 |
| 47.99548 | 1.25E-03 | 6.51E-07 | 1.57E-06 | 1.45E-01 |

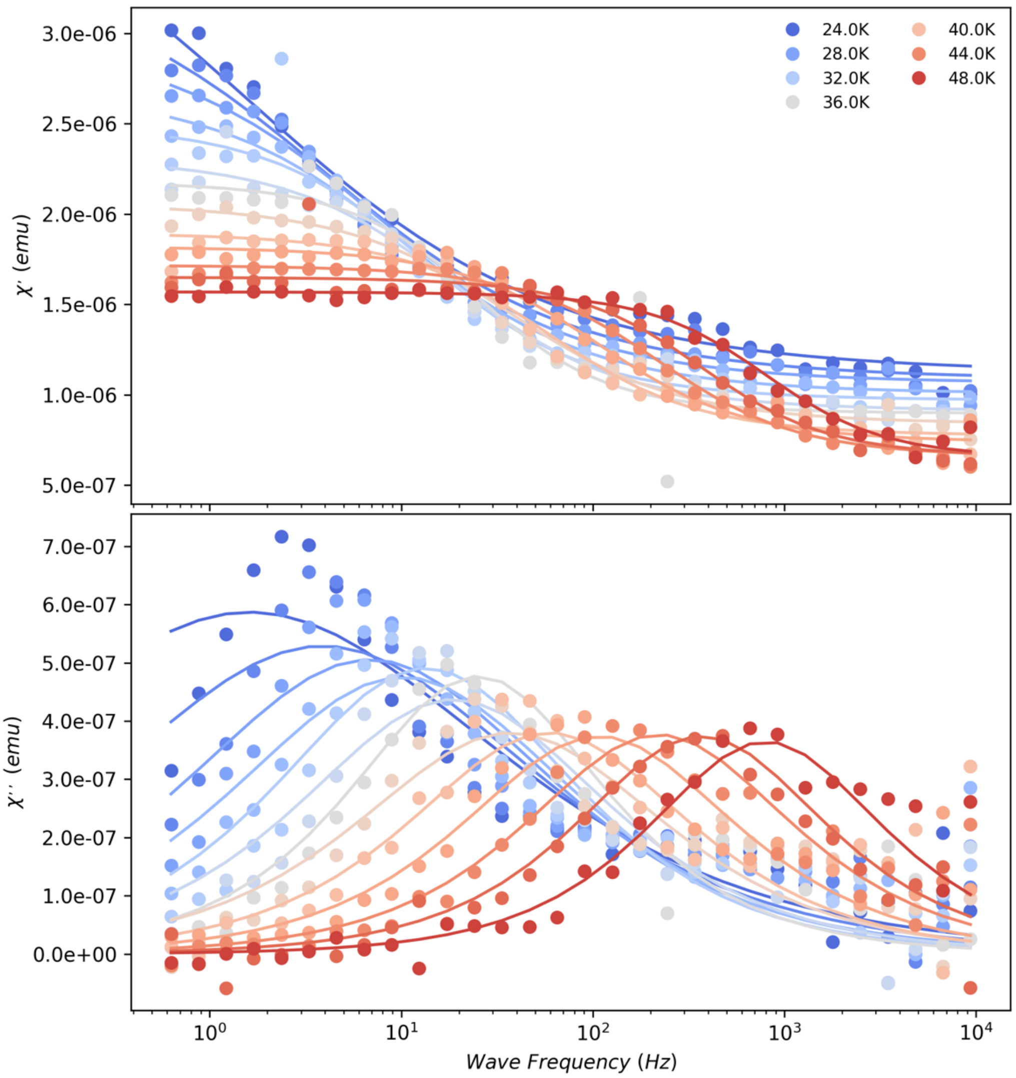


**Figure S2**. AC susceptibility for **1-$^{164}$Dy@Y** recorded under 0 Oe DC field. Points are experimental data, lines are the best fit to the generalised Debye model.

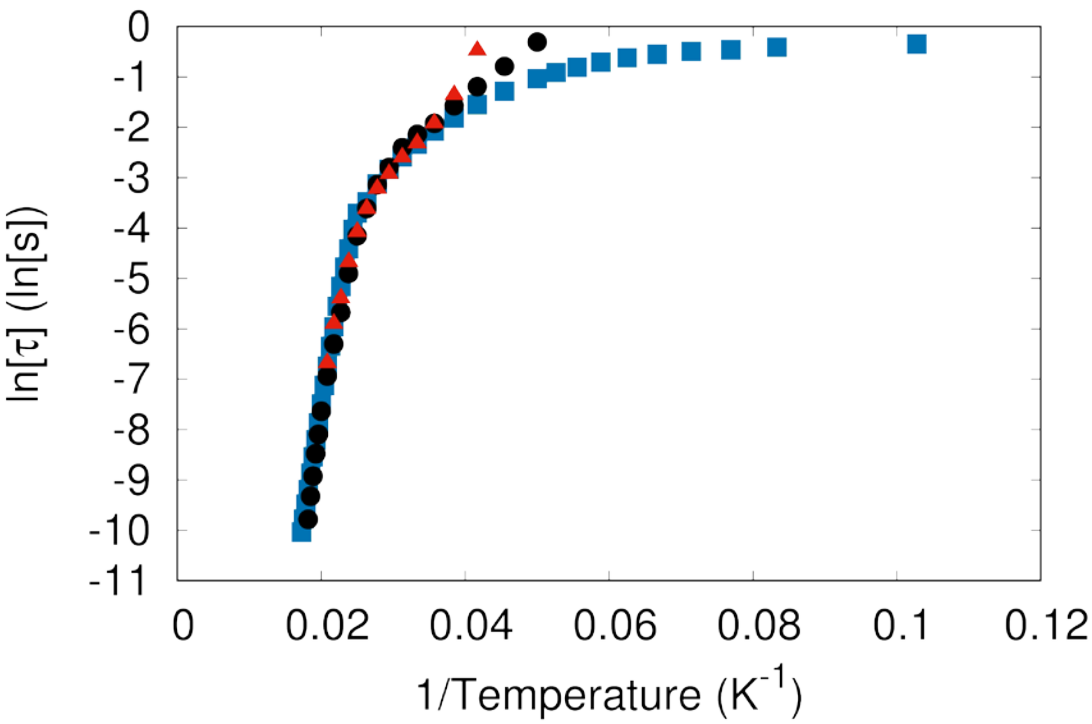


**Figure S3**. Magnetic relaxation rate as a function of temperature for pure natural abundance **1** (blue squares), for its ~5% diluted analogue (black circles) and for its ~5% diluted $^{164}$Dy-enriched analogue (red triangles). Black and blue data sets taken from ref. [8]. Red data from generalised Debye fits of the AC susceptibility data for **1-$^{164}$Dy@Y**.

**Table S2.** Generalised Debye model fit parameters for AC data for **2-$^{164}$Dy@Y**.

| Temperature (K) | τ (s) | $\chi_S$ (emu) | $\chi_T$ (emu) | α |
|---|---|---|---|---|
| 22.00093 | 6.85E-01 | 1.08E-08 | 1.99E-06 | 2.34E-01 |
| 24.00134 | 3.47E-01 | 4.94E-08 | 1.82E-06 | 2.87E-01 |
| 26.0006 | 1.23E-01 | 1.68E-08 | 1.64E-06 | 3.04E-01 |
| 28.00237 | 4.42E-02 | -3.94E-08 | 1.60E-06 | 3.79E-01 |
| 30.00101 | 9.62E-03 | -1.39E-07 | 1.46E-06 | 4.24E-01 |
| 32.00164 | 1.44E-03 | -3.57E-07 | 1.36E-06 | 4.47E-01 |

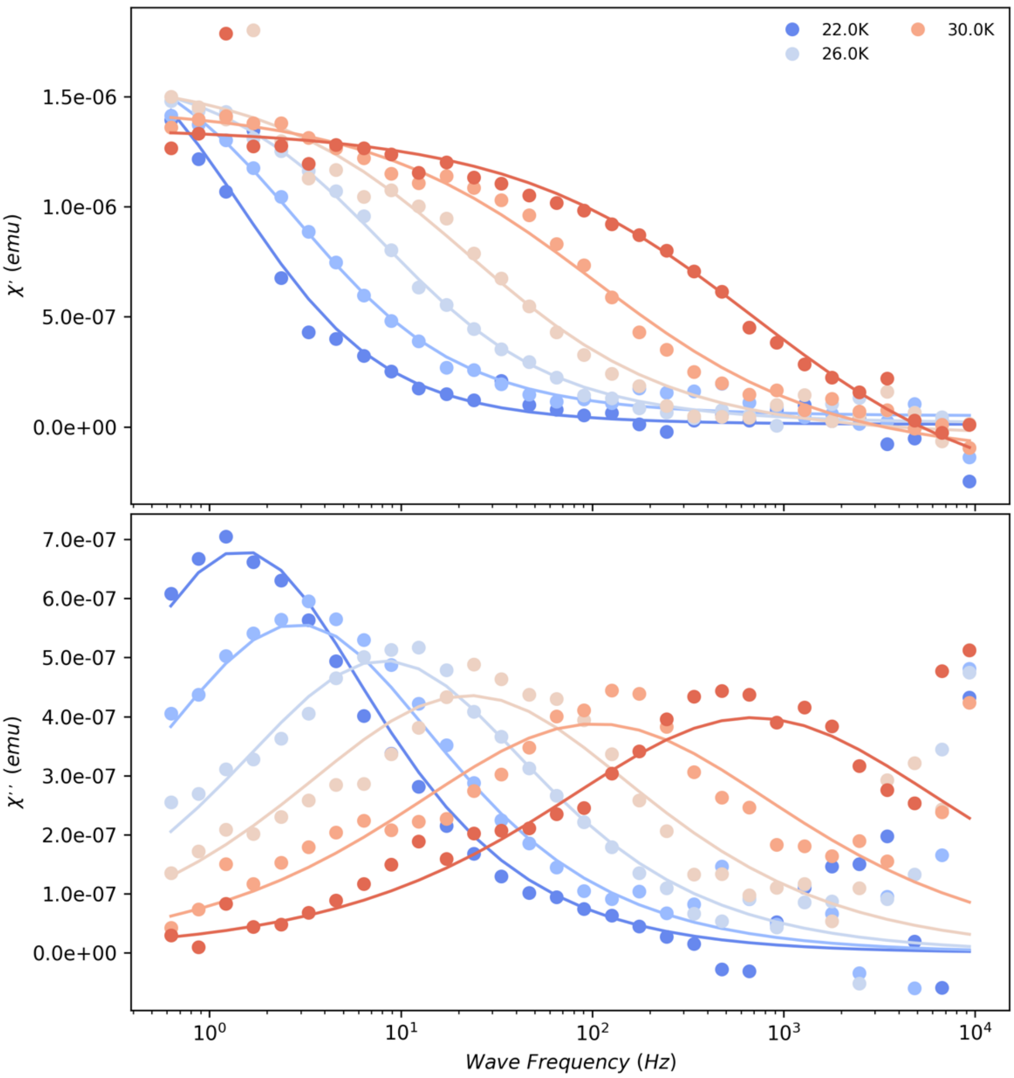


**Figure S4**. AC susceptibility for **2-$^{164}$Dy@Y** recorded under 0 Oe DC field. Points are experimental data, lines are the best fit to the generalised Debye model.

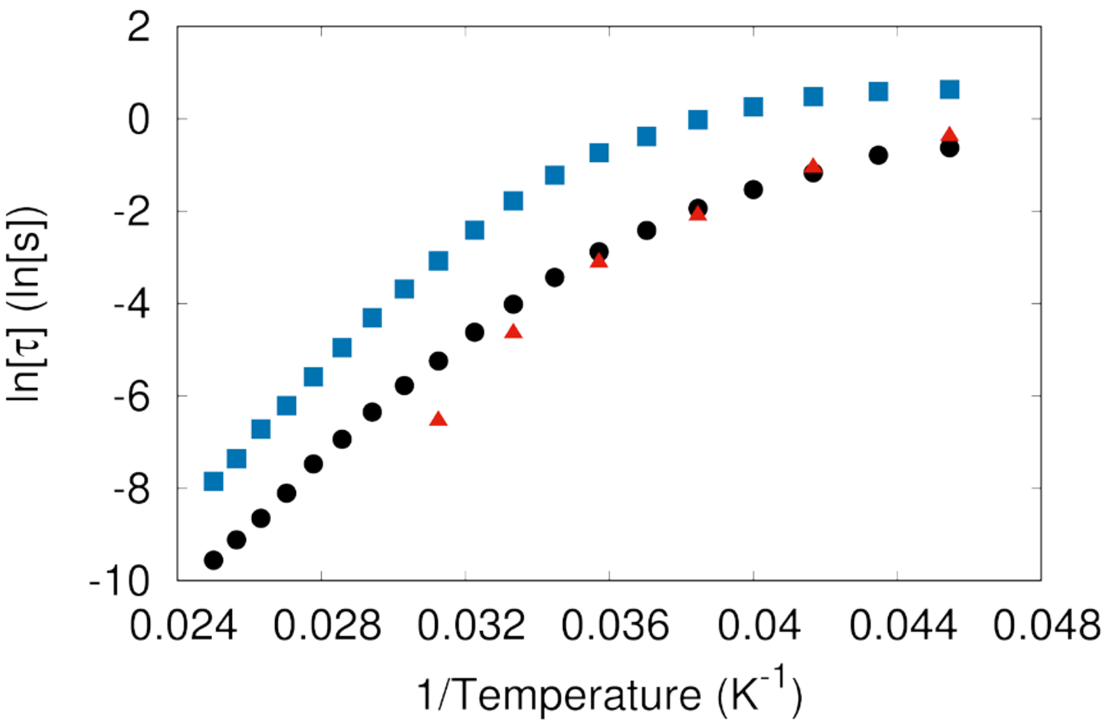


**Figure S5**. Magnetic relaxation rate as a function of temperature for pure natural abundance **2** (blue squares and black circles), and for its ~5% diluted $^{164}$Dy-enriched analogue (red triangles). Black and blue data sets taken from ref. [9]. Red data from generalised Debye fits of the AC susceptibility data for **2-$^{164}$Dy@Y**.

**Table S3.** Generalised Debye model fit parameters for AC data for **3-$^{164}$Dy@Y**.

| Temperature (K) | τ (s) | $\chi_S$ (emu) | $\chi_T$ (emu) | α |
|---|---|---|---|---|
| 71.9986 | 5.19E-01 | -3.04E-08 | 1.06E-06 | 4.73E-02 |
| 74.00098 | 2.90E-01 | -2.59E-08 | 1.02E-06 | 5.40E-02 |
| 75.99788 | 1.65E-01 | -2.79E-08 | 9.83E-07 | 4.82E-02 |
| 78.00023 | 1.19E-01 | -4.10E-08 | 1.04E-06 | 1.16E-01 |
| 80.00066 | 5.67E-02 | -2.99E-08 | 9.29E-07 | 3.43E-02 |
| 81.9991 | 3.33E-02 | -5.08E-08 | 9.14E-07 | 6.45E-02 |
| 84.00008 | 2.06E-02 | -4.41E-08 | 8.75E-07 | 3.84E-02 |
| 85.99803 | 1.25E-02 | -4.39E-08 | 8.61E-07 | 5.90E-02 |
| 87.99915 | 7.73E-03 | -7.94E-08 | 8.50E-07 | 5.31E-02 |
| 89.99792 | 5.65E-03 | -1.30E-07 | 9.04E-07 | 1.88E-01 |
| 92.00081 | 2.57E-03 | -1.64E-07 | 8.01E-07 | 1.78E-01 |
| 93.99989 | 1.91E-03 | -1.27E-07 | 7.97E-07 | 1.14E-01 |
| 95.99992 | 1.08E-03 | -2.16E-07 | 7.85E-07 | 1.77E-01 |
| 97.99941 | 4.85E-04 | -4.71E-07 | 7.54E-07 | 1.79E-01 |
| 99.99975 | 4.10E-04 | -3.49E-07 | 7.56E-07 | 1.99E-01 |
| 102.0041 | 2.52E-04 | -4.76E-07 | 7.27E-07 | 1.91E-01 |
| 104.0004 | 1.41E-04 | -6.54E-07 | 7.01E-07 | 1.80E-01 |

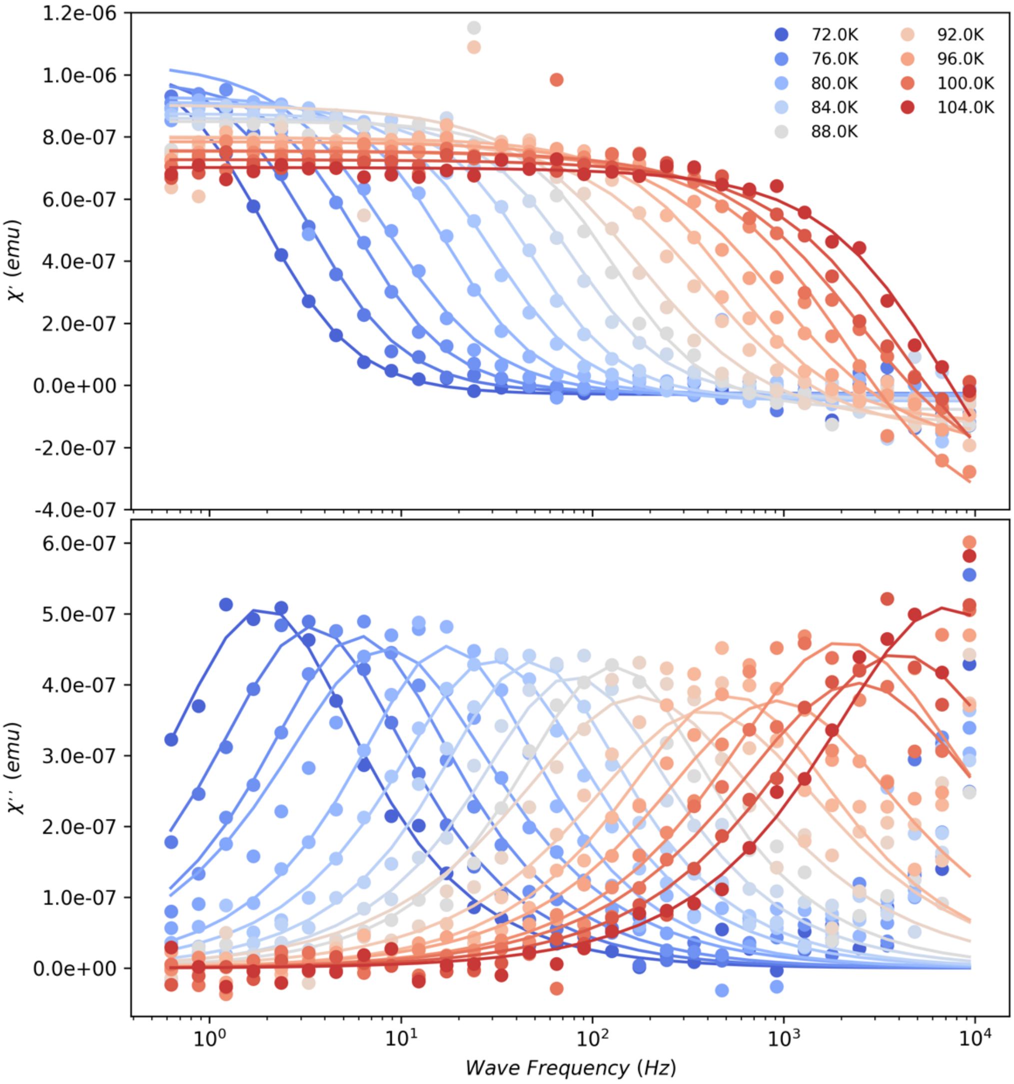


**Figure S6**. AC susceptibility for **3-[164]Dy@Y** recorded under 0 Oe DC field. Points are experimental data, lines are the best fit to the generalised Debye model.

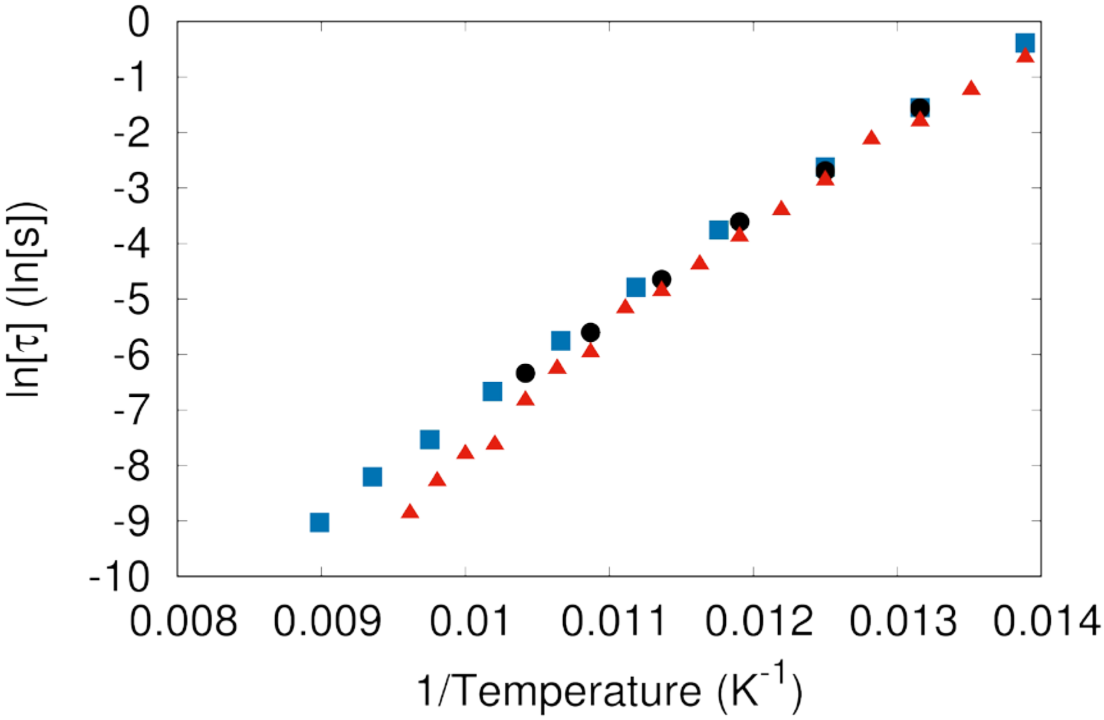


**Figure S7**. Magnetic relaxation rate as a function of temperature for pure natural abundance **3** (blue squares), for its ~5% diluted analogue (black circles) and for its ~5% diluted $^{164}$Dy-enriched analogue (red triangles). Black and blue data sets taken from ref. [12]. Red data from generalised Debye fits of the AC susceptibility data for **3-$^{164}$Dy@Y**.

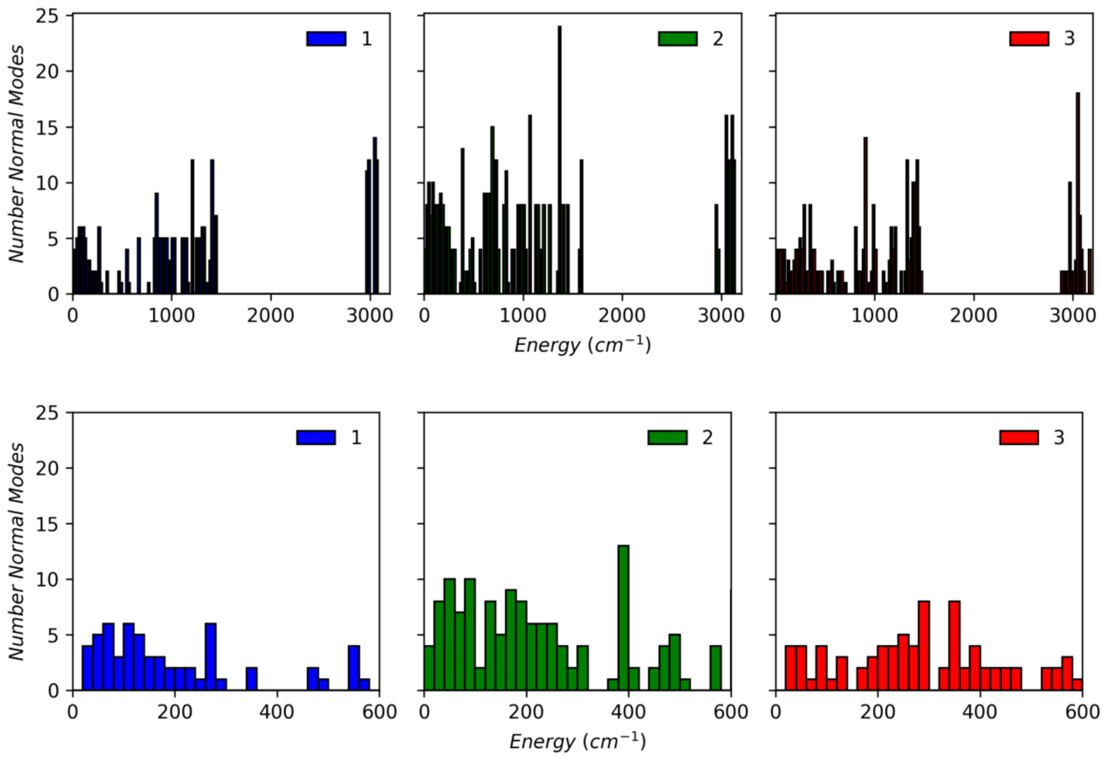


**Figure S8**. Pseudo vibrational density of states for the complex ions in **1** – **3**, with a histogram bin size of 20 cm$^{-1}$. Lower plots are of the low-energy region.

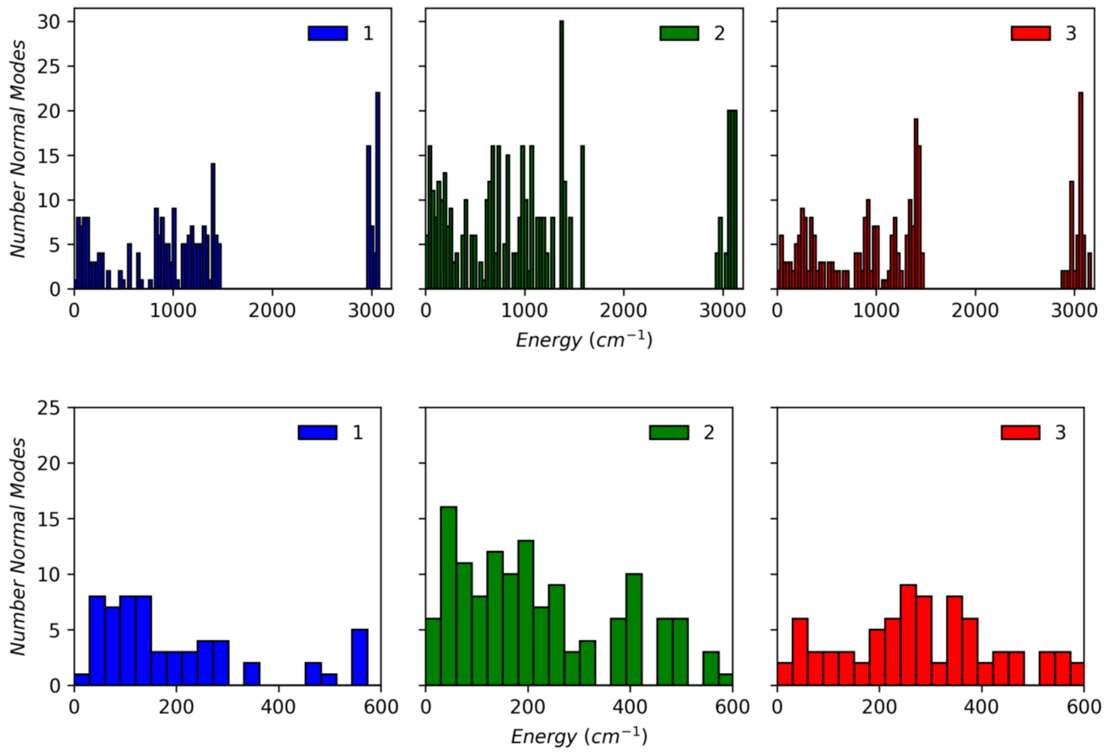


**Figure S9**. Pseudo vibrational density of states for the complex ions in **1** – **3**, with a histogram bin size of 30 cm$^{-1}$. Lower plots are of the low-energy region.

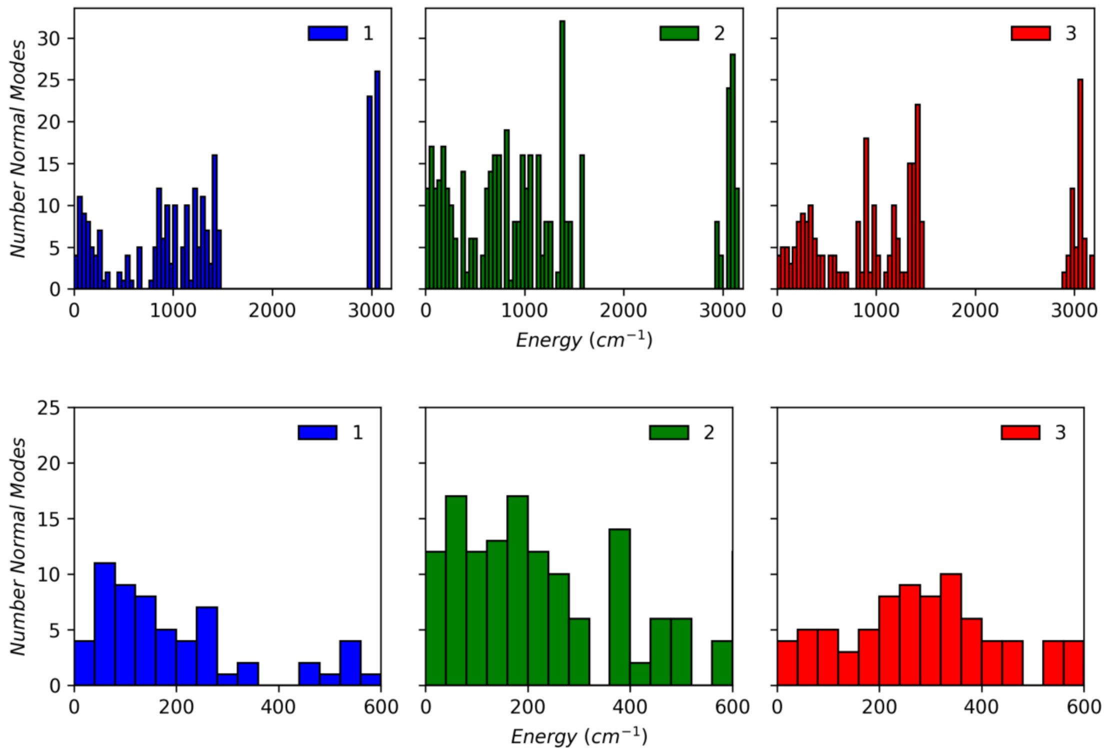


**Figure S10**. Pseudo vibrational density of states for the complex ions in **1 – 3**, with a histogram bin size of 40 cm$^{-1}$. Lower plots are of the low-energy region.

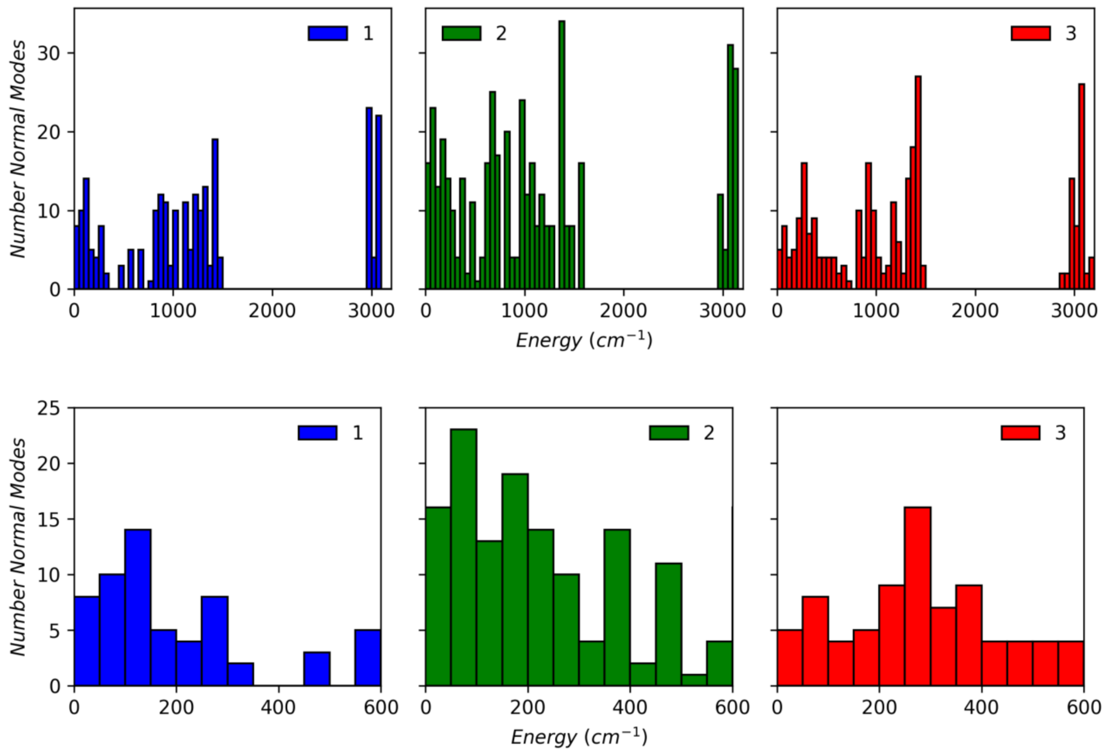


**Figure S11**. Pseudo vibrational density of states for the complex ions in **1 – 3**, with a histogram bin size of 50 cm$^{-1}$. Lower plots are of the low-energy region.

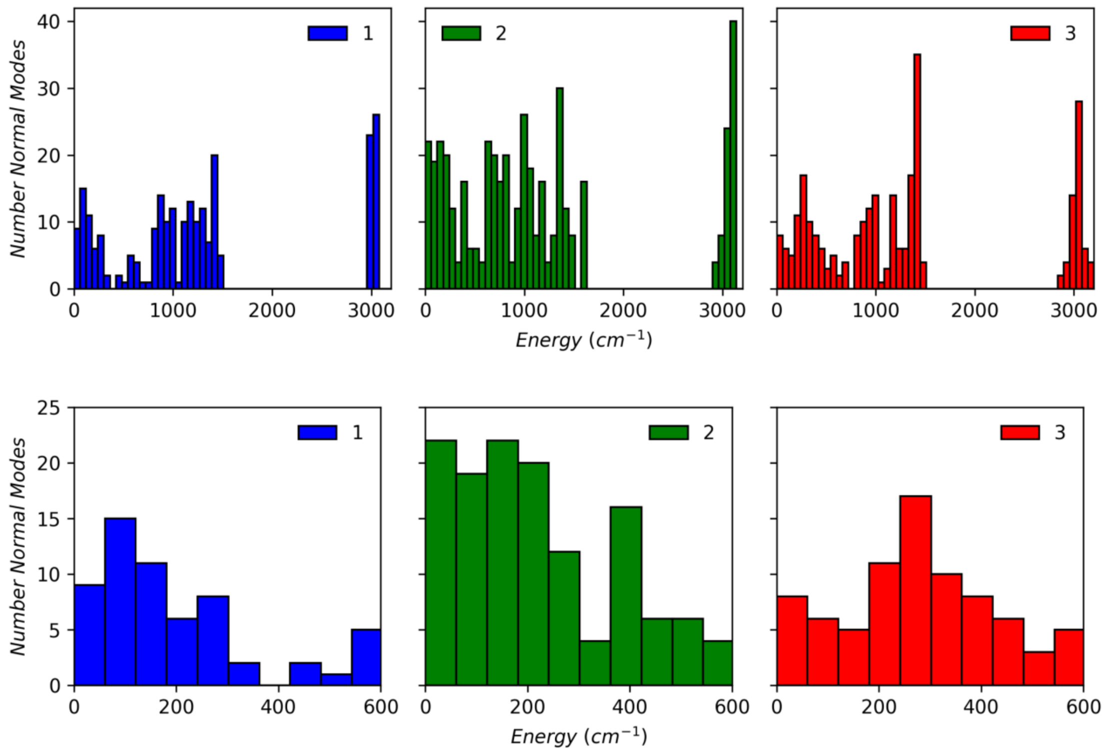


**Figure S12**. Pseudo vibrational density of states for the complex ions in **1 – 3**, with a histogram bin size of 60 $cm^{-1}$. Lower plots are of the low-energy region.

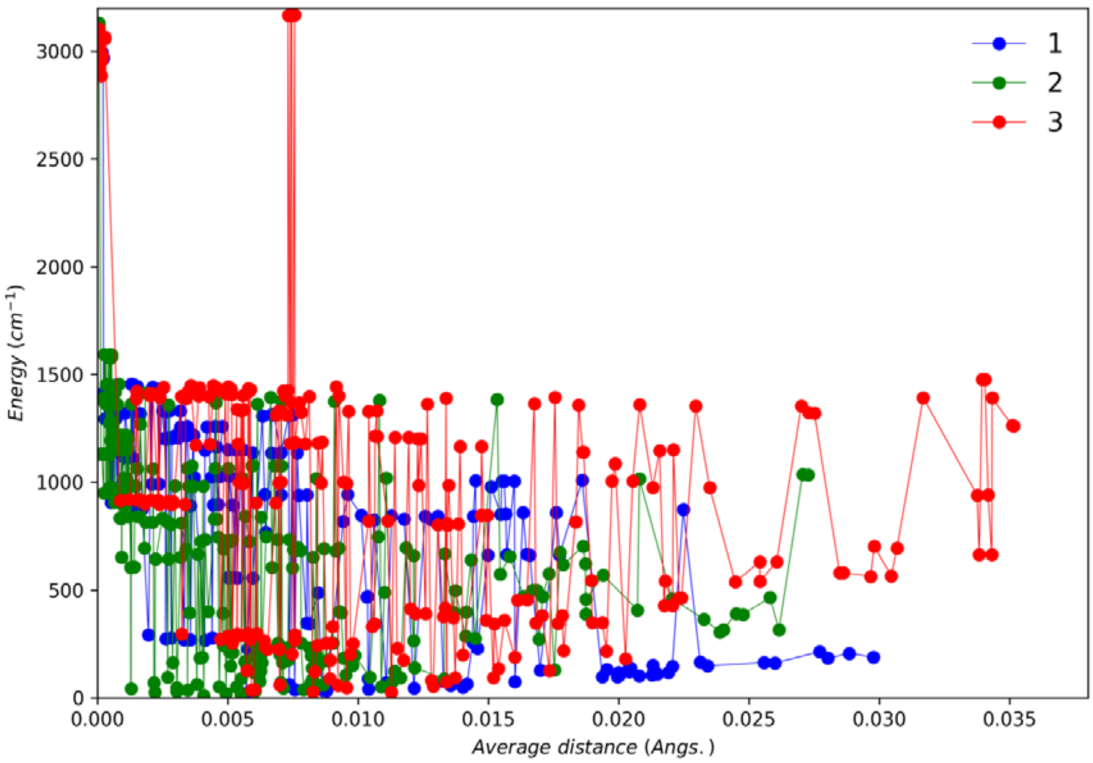


**Figure S13.** Energy of vibrational modes as a function of average displacement of the Dy(III) and first coordination sphere atoms in **1 – 3**.

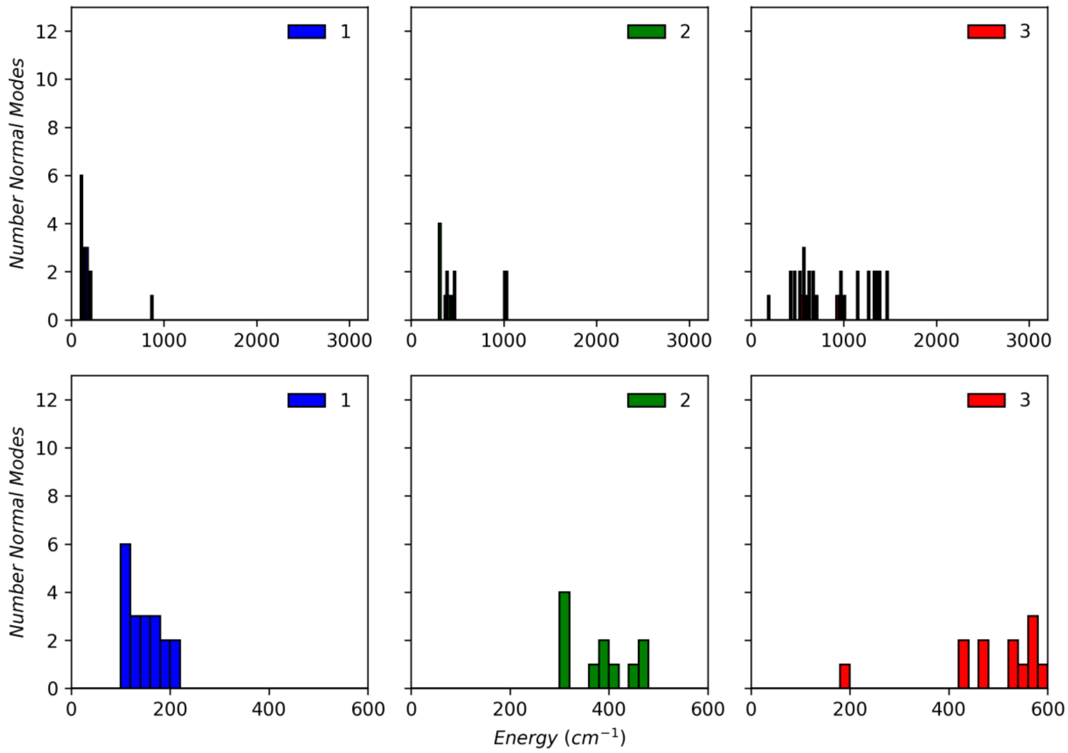


**Figure S14**. Pseudo vibrational density of states for the complex ions in **1 – 3**, only including modes with an average first coordination sphere displacement of ≥ 0.02 Å, with a histogram bin size of 20 $cm^{-1}$. Lower plots are of the low-energy region.

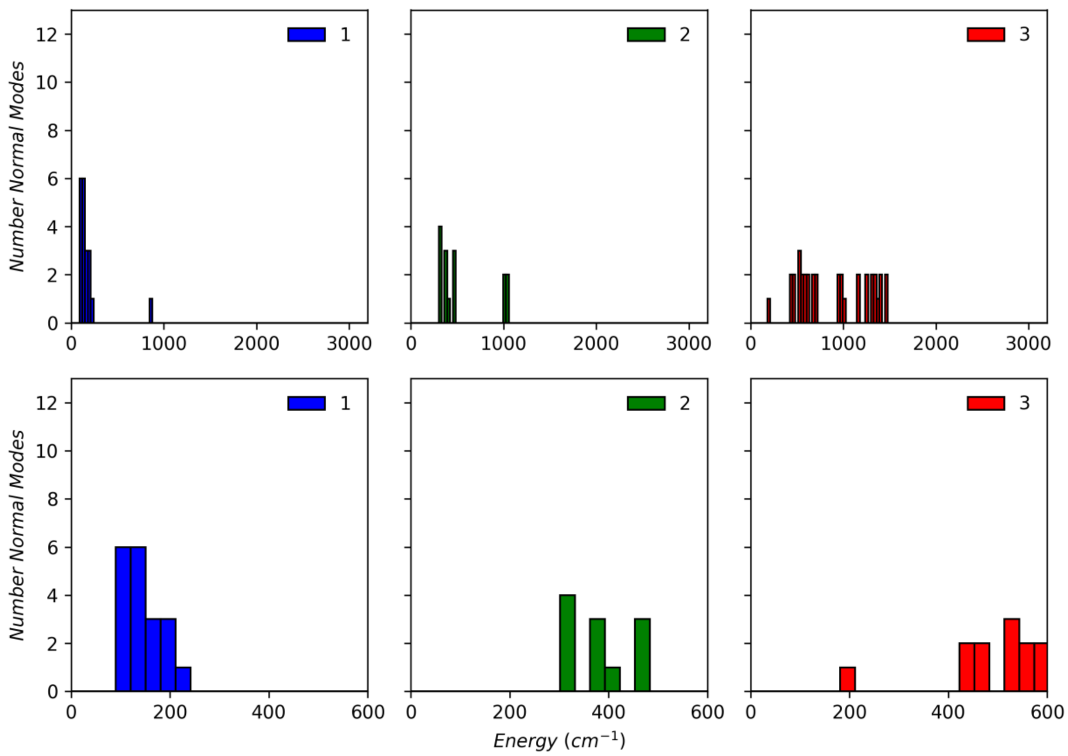


**Figure S15**. Pseudo vibrational density of states for the complex ions in **1 – 3**, only including modes with an average first coordination sphere displacement of ≥ 0.02 Å, with a histogram bin size of 30 $cm^{-1}$. Lower plots are of the low-energy region.

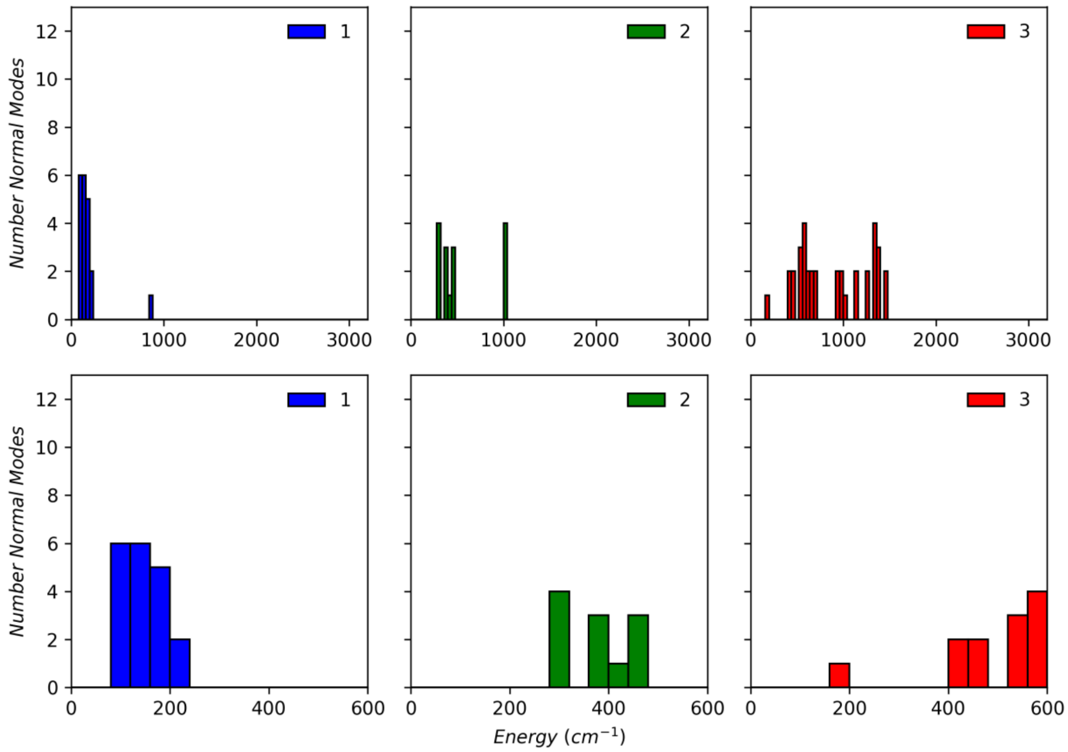


**Figure S16**. Pseudo vibrational density of states for the complex ions in **1 – 3**, only including modes with an average first coordination sphere displacement of ≥ 0.02 Å, with a histogram bin size of 40 $cm^{-1}$. Lower plots are of the low-energy region.

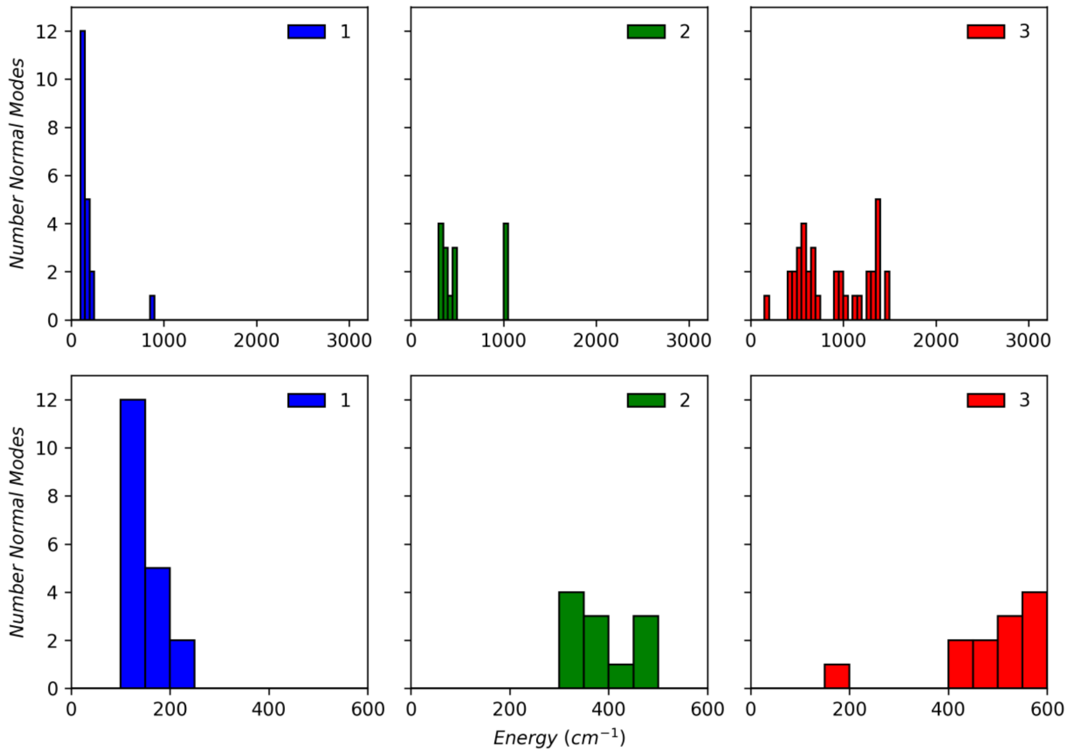


**Figure S17**. Pseudo vibrational density of states for the complex ions in **1 – 3**, only including modes with an average first coordination sphere displacement of ≥ 0.02 Å, with a histogram bin size of 50 $cm^{-1}$. Lower plots are of the low-energy region.

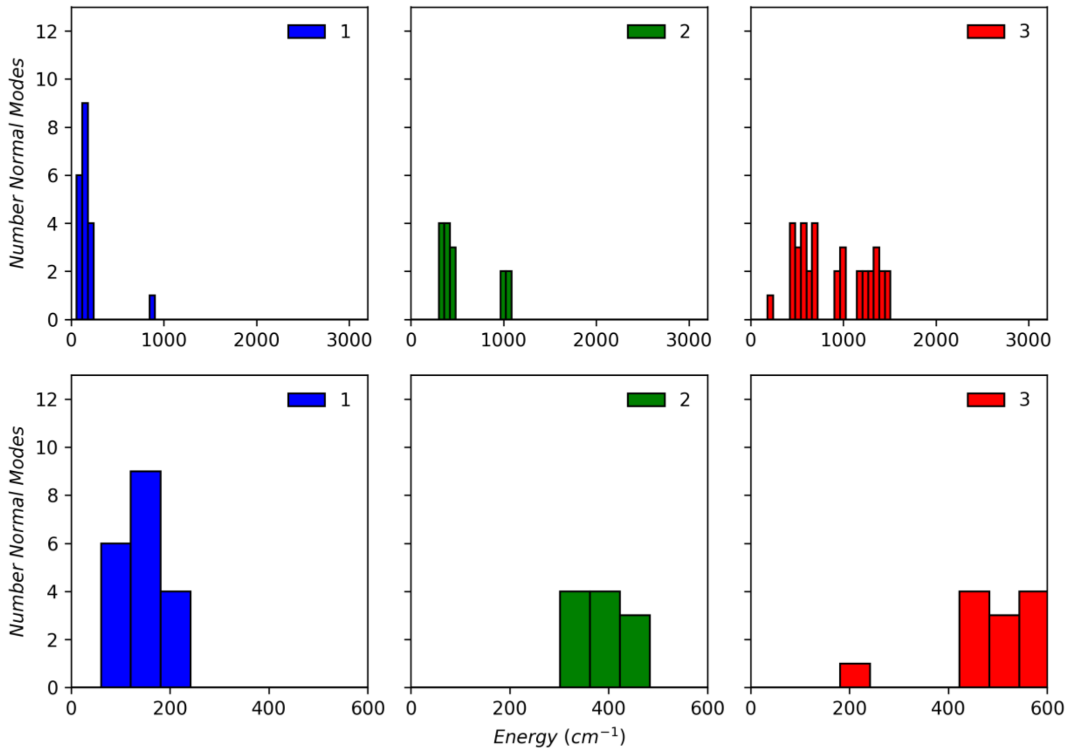


**Figure S18**. Pseudo vibrational density of states for the complex ions in **1 – 3**, only including modes with an average first coordination sphere displacement of ≥ 0.02 Å, with a histogram bin size of 60 $cm^{-1}$. Lower plots are of the low-energy region.

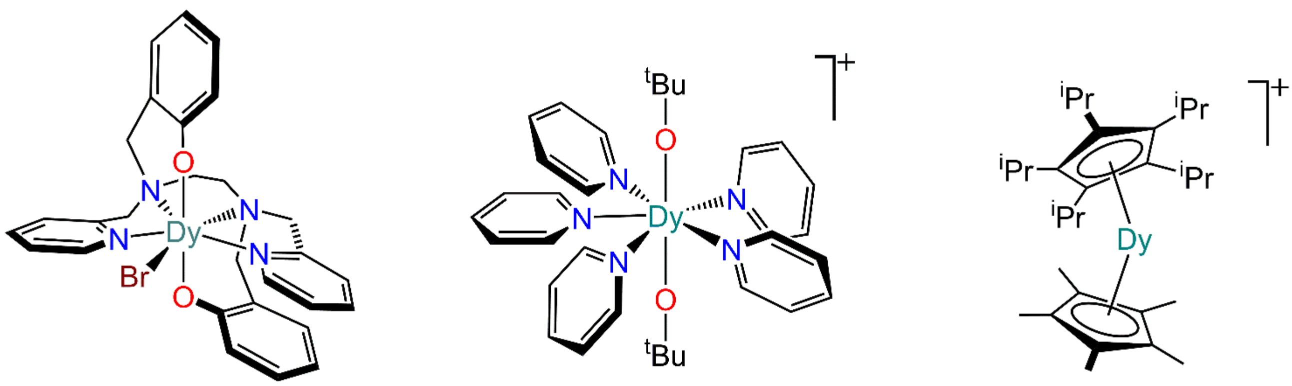


**Figure S19**. Molecular structures of compounds **4**,[22] **5**[23] and **6**.[24]

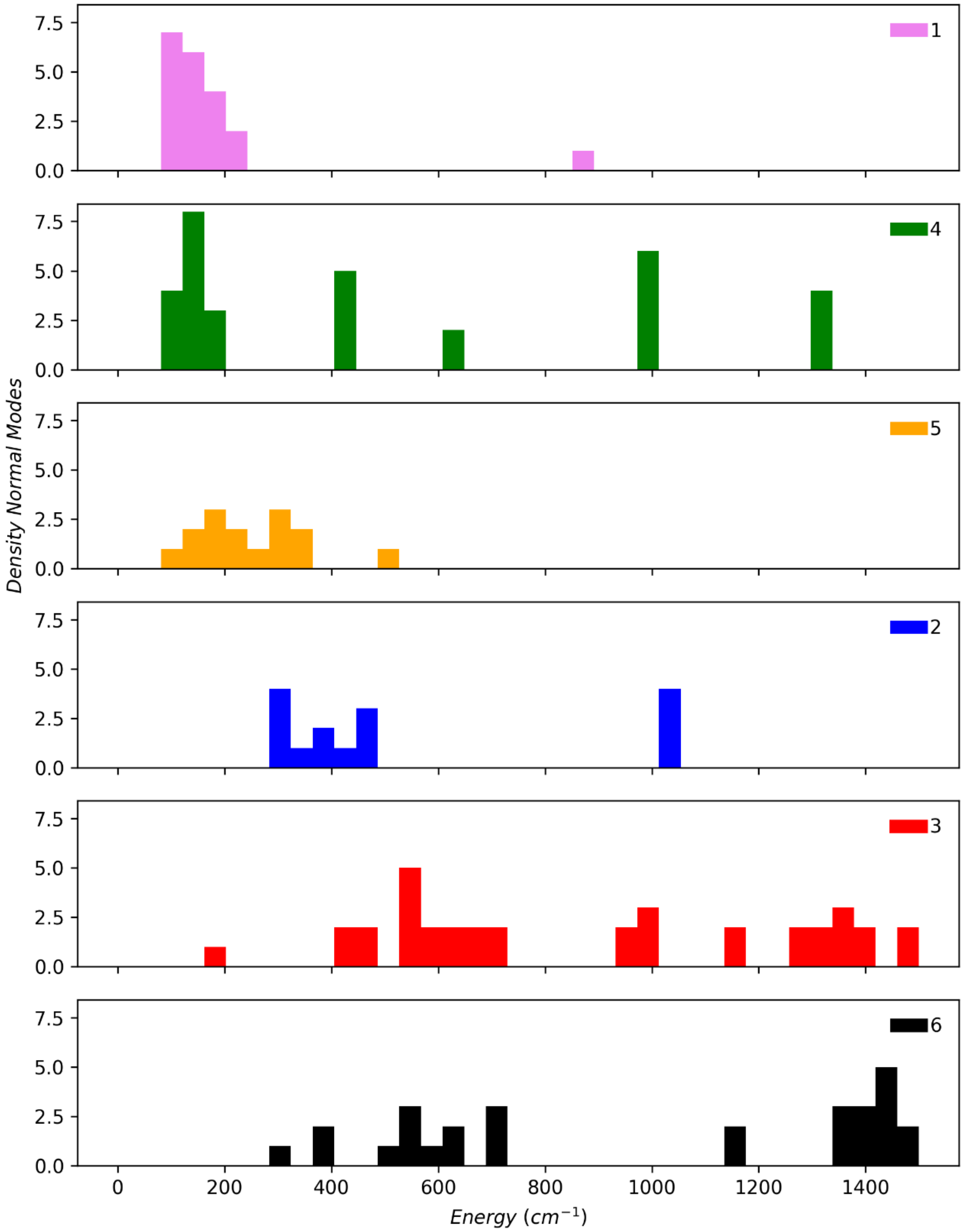


**Figure S20**. Pseudo vibrational density of states for the complex ions in **1 – 6**, only including modes with an average first coordination sphere displacement of ≥ 0.02 Å, with a histogram bin size of 40 $cm^{-1}$.

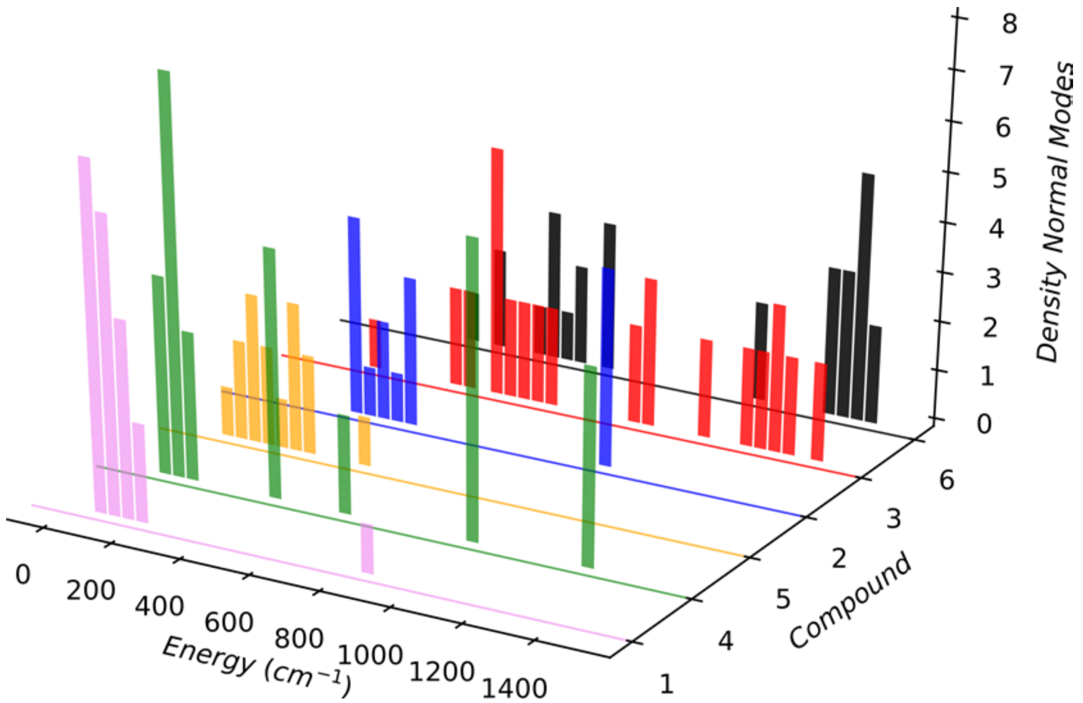


**Figure S21**. Pseudo vibrational density of states for the complex ions in **1 – 6**, only including modes with an average first coordination sphere displacement of ≥ 0.02 Å, with a histogram bin size of 40 $cm^{-1}$.

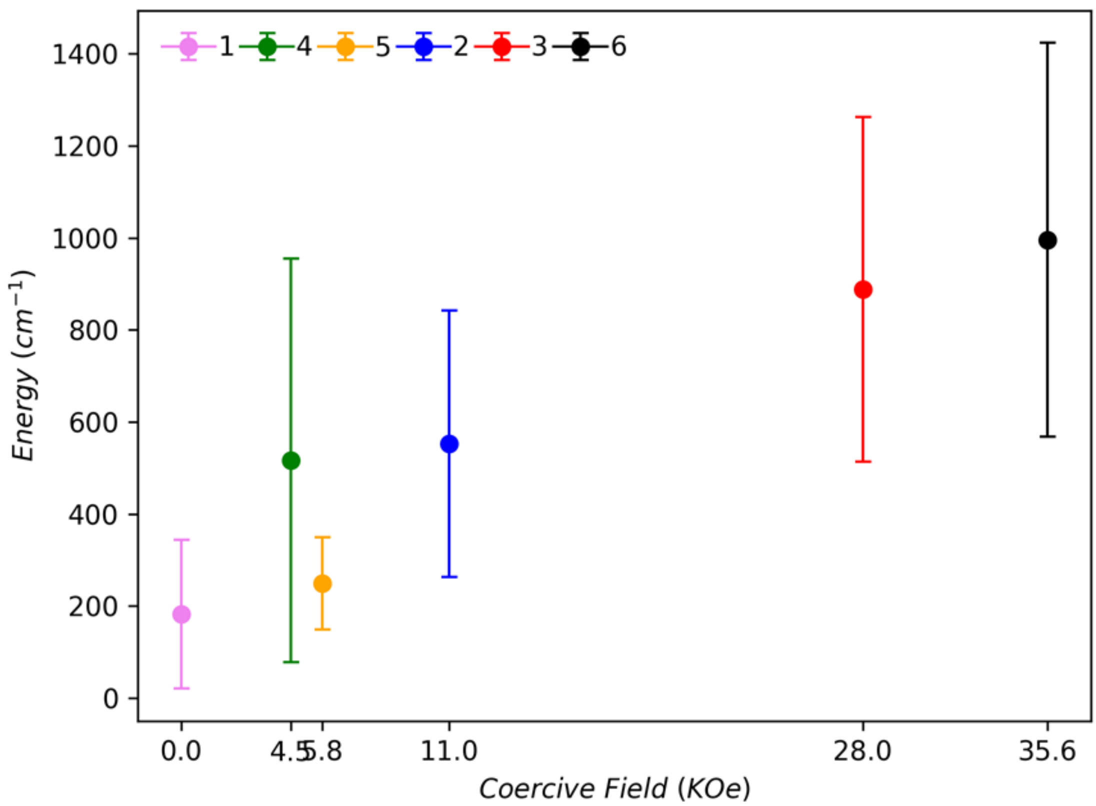


**Figure S22**. Mean and standard deviation (error bars) of the energies of vibrational modes with an average displacement of ≥ 0.02 Å as a function of the coercive field of compounds **1** - **6**. The field sweep rates used to extract the coercive fields are 22, 22, 22, 12, 40, 50 Oe/s, respectively. Compound **4** has too-low a coercive field as it was measured with roughly half the sweep rate of **1 – 3**, while **5** and **6** have too-high a coercive field as it was measured with roughly double the sweep rate of **1 – 3**; that is, if the sweep rates were constant it is likely that the the positions of **4** and **5** should be reversed, thus obeying the trend.

**References**


1 W. Huang, J. L. Brosmer and P. L. Diaconescu, *New J. Chem.*, 2015, **39**, 7696–7702.
2 F. Jaroschik, F. Nief, X.-F. Le Goff and L. Ricard, *Organometallics*, 2007, **26**, 3552–3558.
3 E. S. Stoyanov, I. V. Stoyanova and C. A. Reed, *Chem. – Eur. J.*, 2008, **14**, 7880–7891.
4 J. B. Lambert, S. Zhang and S. M. Ciro, *Organometallics*, 1994, **13**, 2430–2443.
5 M. Schlosser and J. Hartmann, *Angew. Chem. Int. Ed. Engl.*, 1973, **12**, 508–509.
6 R. Appel and I. Ruppert, *Z. Für Anorg. Allg. Chem.*, 1974, **406**, 131–144.
7 W. J. Evans, J. M. Olofson and J. W. Ziller, *J. Am. Chem. Soc.*, 1990, **112**, 2308–2314.
8 Y.-S. Ding, K.-X. Yu, D. Reta, F. Ortu, R. E. P. Winpenny, Y.-Z. Zheng and N. F. Chilton, *Nat. Commun.*, 2018, **9**, 3134.
9 M. Gregson, N. F. Chilton, A.-M. Ariciu, F. Tuna, I. F. Crowe, W. Lewis, A. J. Blake, D. Collison, E. J. L. McInnes, R. E. P. Winpenny and S. T. Liddle, *Chem Sci*, 2016, **7**, 155–165.
10 P. B. Hitchcock, M. F. Lappert, L. Maron and A. V. Protchenko, *Angew. Chem. Int. Ed.*, 2008, **47**, 1488–1491.
11 C. A. P. Goodwin, A. Smith, F. Ortu, I. J. Vitorica-Yrezabal and D. P. Mills, *Dalton Trans.*, 2016, **45**, 6004–6014.
12 C. A. P. Goodwin, F. Ortu, D. Reta, N. F. Chilton and D. P. Mills, *Nature*, 2017, **548**, 439–442.
13
14 J. P. Perdew, K. Burke and M. Ernzerhof, *Phys. Rev. Lett.*, 1996, **77**, 3865–3868.
15 J. P. Perdew, K. Burke and M. Ernzerhof, *Phys. Rev. Lett.*, 1997, **78**, 1396–1396.
16 S. Grimme, *Wiley Interdiscip. Rev. Comput. Mol. Sci.*, 2011, **1**, 211–228.
17 A. Bergner, M. Dolg, W. Küchle, H. Stoll and H. Preuß, *Mol. Phys.*, 1993, **80**, 1431–1441.
18 M. Kaupp, P. v. R. Schleyer, H. Stoll and H. Preuss, *J. Chem. Phys.*, 1991, **94**, 1360–1366.
19 M. Dolg, H. Stoll, H. Preuss and R. M. Pitzer, *J. Phys. Chem.*, 1993, **97**, 5852–5859.
20 T. H. Dunning, *J. Chem. Phys.*, 1989, **90**, 1007–1023.
21 D. E. Woon and T. H. Dunning, *J. Chem. Phys.*, 1993, **98**, 1358–1371.
22 J. Liu, Y.-C. Chen, J.-L. Liu, V. Vieru, L. Ungur, J.-H. Jia, L. F. Chibotaru, Y. Lan, W. Wernsdorfer, S. Gao, X.-M. Chen and M.-L. Tong, *J. Am. Chem. Soc.*, **2016**, *138*, 5441–5450.
23 Y.-S. Ding, N. F. Chilton, R. E. P. Winpenny and Y.-Z. Zheng, *Angew. Chemie Int. Ed.*, **2016**, *55*, 16071–16074.
24 F. Guo, B. M. Day, Y. Chen, M. Tong, A. Mansikkamäki and R. A. Layfield, *Science*, **2018**, *362*, 1400–1403.